Remote Sensing Applications: Society and Environment 10 (2018) 104–119

Contents lists available at ScienceDirect

Remote Sensing Applications: Society and Environment

journal homepage: www.elsevier.com/locate/rsase

Image quality restoration framework for contrast enhancement of satellite remote sensing images

Shilpa Suresh[a], Devikalyan Das[b], Shyam Lal[a,*], Deep Gupta[c]

[a] Department of Electronics and Communication Engineering, National Institute of Technology Karnataka, Surathkal, Mangaluru 575025, Karnataka, India
[b] Department of Electronics and Telecommunication Engineering, Veer Surendra Sai University of Technology, Burla, Sambalpur 768018, Odisha, India
[c] Department of Electronics and Communication Engineering, Vishvasaraya National Institute of Technology, Nagpur, Maharashtra, India

ARTICLE INFO

Keywords:
Remote sensing
Contrast
Restoration
Quality

ABSTRACT

Researches in satellite remote sensing images mainly revolves around enhancement of contrast and removal of noise in image, which affects the data comprehensibility and clarity. Hence, it is always a challenge to process the satellite remote sensing images in order to obtain better quality images with enhanced visibility and minimum image artifacts for improving their application value. In this paper, an effective quality enhancement framework is proposed, which mainly focuses on contrast enhancement of satellite remote sensing images. Several satellite remote sensing images were tested to ratify the effectiveness of the proposed method over other existing remote sensing enhancement methods and their quantitative results are borne out by NIQMC (No Reference Image Quality Metric for Contrast distortion), BIQME (Blind Image Quality Measure of Enhanced images), MICHELSON (Michelson Contrast), DE (Discrete Entropy), EME (Measure of enhancement) and PIXDIST (Pixel distance) along with qualitative results comparison. Results depict that the visual enhancement obtained using the proposed method is superior to other existing enhancement methods. Finally, the simulation results unveil that proposed method is effective and efficient for satellite remotes sensing images.

1. Introduction

Satellite remote sensing images are popularly used in multifarious disciplines like space and geoscience departments, agriculture for crop identification, crop area determination and crop condition monitoring, and other humanitarian applications (Cheng et al., 2015; Zhang et al., 2015). But these images are often tarnished in terms of visual quality owing to various factors like the environmental noises and other intermeddling factors during their acquisition. So, processing and analysis of these images are necessary to facilitate amelioration in the visual attributes of these images. Image contrast is one of the important visual attributes which provide significant contribution to the image quality. Since the sensitivities of human visual system are more towards the image contrast as compared to absolute luminance, it is seen as the difference in the color and brightness of the objects. Low-contrast regions are darker and regions owing to high contrast are visible as artificially illuminated. Hence, both will lead to loss of significant information. So, the challenge is to optimally enhance the image contrast so as to improve the visibility, and at the same time preserving the information present in the input image. Hence, image enhancement is a rudimentary step in all digital image processing and analysis applications, which improves the interpretability or information perceived by humans.

Furthermore, a satellite sensor must capture a very wide range of scenes from different location on the earth surfaces, from very low radiance (i.e. oceans, low solar elevation angles, high latitudes) to very high radiance (i.e. snow, sand, high solar elevation angles, and low latitudes) (Schowengerdt, 1997; Lisani et al., 2016). As a result, the quantization can be coarse, and any given satellite image will generally occupy only a limited portion of the available dynamic range, therefore having low contrast (Lisani et al., 2016). Moreover, the energy reaching the satellite must pass through the entire depth of the Earth's atmosphere. Atmospheric effects may also reduce the dynamic range of the satellite image (Lisani et al., 2016). Hence, representation of these satellite images to human observers analytically requires the use of a remote sensing contrast enhancement method.

The most basic image enhancement method is histogram equalization as its implementation is very simple. But it always results in over enhanced images or scarce detail preservation (Chen et al., 2016; Arici et al., 2003; Sen and Pal, 2011; Wu, 2011; Celik and Tjahjadi, 2012; Xu et al., 2014). The enhancements due to transform domain methods mainly deal with contrast magnification or enhancement of high

* Corresponding author.
E-mail addresses: ec14f13.shilpa@nitk.edu.in (S. Suresh), devikalyandas9067@gmail.com (D. Das), shyamfec@nitk.edu.in (S. Lal), deepgupta@ece.vnit.ac.in (D. Gupta).

https://doi.org/10.1016/j.rsase.2018.03.008
Received 2 December 2017; Received in revised form 16 March 2018; Accepted 22 March 2018
Available online 27 March 2018
2352-9385/ © 2018 Elsevier B.V. All rights reserved.

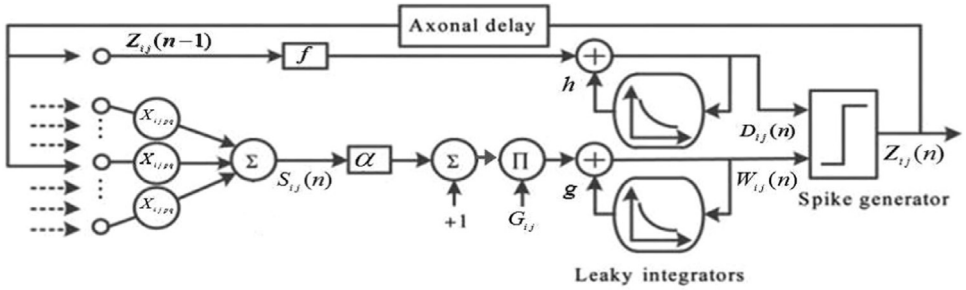

Fig. 1. Schematic of modified linking synaptic computation network.

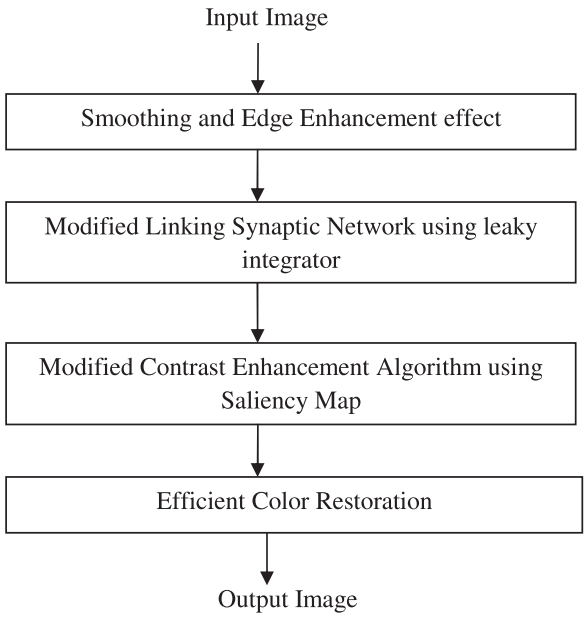

Fig. 2. Workflow diagram of proposed framework.

frequency sub-band coefficients (Starck et al., 2003; Tang et al., 2004; Mukherjee and Mitra, 2008). But, sometimes the parameters of these methods are incompetent for satellite images and hence lead to the magnification of noise intensity. The tone mapping methods often remain under-enhanced and appear faded because of compression of luminance values. The linking models (Zhan et al., 2017, 2016) often fail in case of satellite images. This is because of excessive smoothing which leads to the loss of certain image information. In the recent years, some of the researchers have also developed new methods for contrast enhancement of remote sensing images (Fu et al., 2015; Lisani et al., 2016; Suresh and Lal, 2017; Li et al., 2017).

The main contributions of this manuscript are given as follows:

- The modified linking synaptic computation network is proposed by remodeling thresholding condition in the linking synaptic computation network proposed by Zhan et al. (2017). This modification helps in reducing computational complexity of the network.
- A robust image quality restoration framework is proposed for contrast enhancement of satellite remote sensing images.

The rest of the paper is organized as follows. In Section 2, the proposed framework is detailed in four sections. The experimental results are presented in Section 3, which demonstrates the efficiency of the proposed method with the state-of-the-art algorithms both qualitatively and quantitatively. Here, a detailed comparison on computational cost is also presented. Finally, Section 4 concludes the discussion by emphasizing the merits and applications of the proposed method.

2. Proposed framework

This section presents detailed analysis of the proposed image quality restoration framework. For an input color image, the enhancement is carried out after converting the image into HSV color space. The color space conversion is included because of its direct relationship with the human visual perception (Vadivel et al., 2005). The proposed approach is delineated in four steps: (1) Smoothing and Edge Enhancement Effect, (2) Modified Linking Synaptic Network using leaky integrator, (3) Modified Contrast Enhancement Algorithm using Saliency Map (4) Efficient Color Restoration after converting the image back to the RGB color space.

Table 1
Performance comparison of different enhancement techniques for image 1.

IMAGE	ALGORITHM	METRICES					
		NIQMC	**BIQME**	**MICHELSON**	**DE**	**EME**	**PIXDIST**
IMG 1	BPDFHE	4.9882	0.6019	0.3195	7.4099	69.5518	25.171
	DWT-SVD	5.4135	0.5872	0.1489	7.5678	32.9736	27.9036
	RHE-DCT	5.0853	0.6049	0.2872	7.3772	81.8576	23.9813
	DRAGO	4.4057	0.4262	0.044	6.9558	27.8757	18.364
	DURAND	2.5409	0.2532	0.0189	5.3578	21.5598	10.8651
	FATTAL	4.8072	0.4907	0.0989	7.1809	24.3886	20.6296
	LCC	4.6754	0.52	0.174	7.0638	59.6047	19.6953
	MAI	5.3717	0.552	0.1598	7.3482	44.8579	27.4789
	MSR	4.5923	0.511	0.11	7.2257	47.8007	22.8061
	MSRACE	4.3406	0.4695	0.0678	7.0673	27.2983	20.0358
	FLM	5.089	0.5252	0.35	7.4011	94.6098	26.8297
	LSCN	5.1197	0.5432	0.3186	7.4286	92.8292	25.4777
	JEI	5.5505	0.6385	0.2957	7.742	69.9834	31.1606
	MDE	5.3371	0.562	0.1805	7.6255	35.4652	28.2798
	PROPOSED	**5.8507**	**0.6689**	**0.5168**	**7.9198**	**110.6407**	**38.7609**

Table 2
Performance comparison of different enhancement techniques for image 2.

Image	Algorithm	Metrices					
		NIQMC	**BIQME**	**MICHELSON**	**DE**	**EME**	**PIXDIST**
	BPDFHE	4.0447	0.4225	0.3513	6.6859	58.9631	18.698
	DWT-SVD	5.4073	0.6738	0.1248	7.6669	15.6485	39.3355
	RHE-DCT	5.3954	0.5921	0.2897	7.4791	84.564	30.9496
	DRAGO	4.4605	0.4322	0.014	7.1843	9.5228	23.0223
	DURAND	2.3765	0.2657	0.001	5.5031	4.8172	9.4618
	FATTAL	4.5985	0.4618	0.0922	7.1168	21.2024	19.7041
	LCC	5.0201	0.6006	0.2194	7.3642	49.5128	25.2852
IMG 2	MAI	5.5715	0.6203	0.1389	7.1918	29.2489	36.3566
	MSR	5.1672	0.537	0.1436	7.4687	53.0646	25.2534
	MSRACE	4.9827	0.5262	0.0717	7.5814	23.2005	27.9591
	FLM	5.5063	0.6068	0.4061	7.7009	91.9706	33.0901
	LSCN	5.2999	0.6151	0.3474	7.5532	81.3023	28.921
	JEI	4.8859	0.5672	0.1381	7.4139	40.606	26.8568
	MDE	5.3036	0.6111	0.1234	7.6137	18.312	29.7167
	PROPOSED	**5.793**	**0.6874**	**0.425**	**7.8967**	**99.7892**	**40.1772**

Table 3
Performance comparison of different enhancement techniques for image 3.

Image	Algorithm	Metrices					
		NIQMC	**BIQME**	**MICHELSON**	**DE**	**EME**	**PIXDIST**
	BPDFHE	3.8236	0.4486	0.5026	6.861	67.5585	17.3993
	DWT-SVD	3.6843	0.4195	0.0075	6.8107	11.491	15.6810
	RHE-DCT	3.9025	0.5726	0.1919	6.8537	48.8679	16.2518
	DRAGO	2.9794	0.3185	0.0007	6.4215	7.0793	12.5181
	DURAND	2.9828	0.3267	0.0003	5.5760	5.9766	12.5713
	FATTAL	4.0962	0.4629	0.0352	7.0140	20.8590	18.0277
	LCC	3.7525	0.4652	0.0892	7.0239	40.7108	18.6426
IMG 3	MAI	4.8747	0.5634	0.1343	6.6856	32.9930	26.8252
	MSR	4.3938	0.5041	0.0818	7.2548	39.4527	21.5022
	MSRACE	3.8955	0.4380	0.0368	7.0492	22.4986	18.3555
	FLM	4.7756	0.5729	0.3448	7.4280	80.8634	24.1947
	LSCN	4.8038	0.5866	0.3738	7.4499	78.3596	24.5955
	JEI	3.8086	0.5243	0.0993	6.8849	26.9086	16.3117
	MDE	4.1667	0.4738	0.0181	7.2452	13.7051	21.7447
	PROPOSED	**5.5823**	**0.6881**	**0.6545**	**7.8388**	**125.6491**	**34.3611**

Table 4
Performance comparison of different enhancement techniques for image 4.

Image	Algorithm	Metrices					
		NIQMC	**BIQME**	**MICHELSON**	**DE**	**EME**	**PIXDIST**
	BPDFHE	5.372	0.6339	0.3459	7.6574	71.1923	30.6415
	DWT-SVD	5.6154	0.6355	0.1516	7.7463	38.5349	32.5218
	RHE-DCT	5.5704	0.6576	0.3414	7.7353	95.5908	31.8051
	DRAGO	4.7198	0.458	0.0389	7.1368	24.1236	20.1667
	DURAND	2.485-	0.2915	0.0094	5.0959	14.8056	9.3552
	FATTAL	4.8985	0.5022	0.0536	7.3266	24.5803	22.3571
	LCC	4.9942	0.5333	0.1297	7.3130	47.1736	22.6195
IMG 4	MAI	5.445-	0.5556	0.1031	7.5200	35.4760	28.3791
	MSR	4.5455	0.4779	0.0563	6.9925	36.2279	19.1907
	MSRACE	4.2421	0.4252	0.0306	6.7404	19.9179	15.9037
	FLM	5.2902	0.5753	0.3588	7.5704	82.4718	28.7169
	LSCN	5.5586	0.6004	0.3742	7.7332	95.1383	30.7389
	JEI	5.5792	0.6423	0.2530	7.7554	66.1776	31.2138
	MDE	5.5586	0.6004	0.3742	7.7332	95.1383	30.7389
	PROPOSED	**5.9524**	**0.6959**	**0.6083**	**7.9467**	**116.4518**	**42.138**

2.1. Smoothing and edge enhancement effect

The input image $G_{i,j}$ after conversion to HSV color space is normalized and passed through a guided smoothing filter (He et al., 2013). The filter modifies the details in the image, which is given Eq. (1).

$$E_{i,j} = \varepsilon\ (\overline{G_{i,j}} - G_{i,j})\ (1 - G_{i,j}) \quad (1)$$

Where parameter $G_{i,j}$ is the normalized input image and its magnitude value always less than 1 and the constant ε is mainly used for checking the magnitude of the image details. The value of parameter ε is set as 8 to control the magnitude of the details within the image for all the test images, since it gave better enhancement results (Mukherjee and Mitra,

Table 5
Performance comparison of different enhancement techniques for image 5.

Image	Algorithm	Metrices					
		NIQMC	**BIQME**	**MICHELSON**	**DE**	**EME**	**PIXDIST**
	BPDFHE	5.6084	0.6735	0.1739	7.7896	53.2016	33.9439
	DWT-SVD	5.0772	0.6136	0.0856	7.4767	18.6504	33.8011
	RHE-DCT	5.4995	0.685	0.1586	7.7652	43.1434	35.4589
	DRAGO	4.2793	0.4309	0.0161	7.1513	10.4708	21.5722
	DURAND	2.7599	0.3013	0.0019	5.1885	6.8637	10.5106
	FATTAL	4.5038	0.4663	0.0412	7.0782	18.5127	18.7003
	LCC	5.0449	0.5597	0.1192	7.3810	47.2963	26.1644
IMG 5	MAI	5.5405	0.6109	0.0961	7.6540	28.3446	33.6412
	MSR	5.1564	0.5042	0.0781	7.3028	42.0054	22.6509
	MSRACE	4.7641	0.4641	0.0332	7.1997	19.5319	21.9618
	FLM	5.2932	0.6142	0.3583	7.6426	93.0667	33.7422
	LSCN	5.5804	0.6597	0.3217	7.7900	92.6832	34.8323
	JEI	5.6771	0.6897	0.1689	7.8268	41.8604	40.0066
	MDE	5.5897	0.6904	**0.5371**	7.7397	**130.7856**	37.5939
	PROPOSED	**5.7604**	**0.7067**	0.4352	**7.8412**	99.8586	**42.561**

Table 6
Performance comparison of different enhancement techniques for image 6.

Image	Algorithm	Metrices					
		NIQMC	**BIQME**	**MICHELSON**	**DE**	**EME**	**PIXDIST**
	BPDFHE	5.6389	0.6407	0.2718	7.7843	63.8734	32.3593
	DWT-SVD	5.3929	0.5716	0.0922	7.6833	19.5602	31.7046
	RHE-DCT	5.7814	0.6676	0.4458	7.8215	**120.1166**	36.8432
	DRAGO	5.3138	0.5348	0.1021	7.5185	17.975	29.2791
	DURAND	4.737	0.4897	0.0705	5.6372	16.8364	23.6735
	FATTAL	5.1536	0.5214	0.1767	7.4305	24.4038	24.0966
	LCC	5.4104	0.5717	0.2606	7.5341	63.1146	26.5717
IMG 6	MAI	5.8007	0.6051	0.3039	7.7564	44.3164	36.8138
	MSR	5.5706	0.574	0.2935	7.5961	53.8986	29.6528
	MSRACE	5.5351	0.5643	0.2354	7.6725	36.1679	31.0479
	FLM	5.5615	0.6000	0.4764	7.6769	100.0563	33.6338
	LSCN	5.7001	0.6297	0.4613	7.8176	106.4801	34.772
	JEI	5.8165	0.6563	0.3302	7.9292	47.5987	37.9855
	MDE	5.5862	0.592	0.2858	7.7748	36.8521	33.3646
	PROPOSED	**5.9119**	**0.6851**	**0.5592**	**7.9438**	110.4496	**42.7876**

Table 7
Performance comparison of different enhancement techniques for image 7.

Image	Algorithm	Metrices					
		NIQMC	**BIQME**	**MICHELSON**	**DE**	**EME**	**PIXDIST**
	BPDFHE	4.141	0.4692	0.3583	6.9711	97.7567	19.6191
	DWT-SVD	4.7132	0.5112	0.0542	7.2208	13.7429	24.8612
	RHE-DCT	4.3532	0.5846	0.1806	6.8233	30.6605	17.8199
	DRAGO	3.7151	0.3932	0.0068	6.6713	8.7335	15.5625
	DURAND	2.5326	0.308	0.0026	5.2097	5.6513	10.3452
	FATTAL	4.4289	0.4575	0.0596	6.949	16.068	17.76
	LCC	4.1738	0.5241	0.1366	6.798	45.3133	17.1564
IMG 7	MAI	5.25	0.5619	0.1431	6.8496	21.6947	27.2059
	MSR	5.0956	0.5296	0.1488	7.1522	47.1204	21.2314
	MSRACE	3.6272	0.3937	0.0075	6.5596	8.7118	14.1775
	FLM	5.2049	0.5621	0.4165	7.4462	97.7275	28.0508
	LSCN	4.9663	0.5606	0.3492	7.2667	77.2373	24.5662
	JEI	4.9423	0.6131	0.2544	7.3319	40.2227	23.2063
	MDE	**5.4054**	**0.6924**	0.4003	**7.5717**	88.0613	**33.1407**
	PROPOSED	5.3747	0.6383	**0.5297**	7.5154	**131.2475**	29.0461

2008). Indices *(i, j)* denotes the pixels co-ordinates and the smoothed image is indicated as $\overline{G_{i,j}}$.

The enhanced details are then added and the processed image is represented as in Eq. (2).

$$D_{i\ ,j} = 1 + E_{i,j} - \min(E_{i,j}) \quad (2)$$

After these enhancing and smoothing effects, the satellite image is processed under a modified linking synaptic network for better enhancement effects.

Table 8
Performance comparison of different enhancement techniques for image 8.

Image	Algorithm	Metrices					
		NIQMC	**BIQME**	**MICHELSON**	**DE**	**EME**	**PIXDIST**
IMG 8	BPDFHE	4.7877	0.5721	0.0362	7.2379	17.4704	22.8409
	DWT-SVD	5.3379	0.6179	0.0058	7.573	8.6556	36.4097
	RHE-DCT	5.068	0.5932	0.0309	7.456	15.9983	27.2048
	DRAGO	5.012	0.493	0.001	7.3878	5.4972	25.1908
	DURAND	4.0682	0.4328	0.0013	5.4393	6.113	18.4982
	FATTAL	4.8914	0.5021	0.01	7.3135	11.2301	22.1673
	LCC	4.3106	0.5389	0.0161	6.9428	14.5156	18.0585
	MAI	5.7268	0.606	0.0244	7.5571	13.9102	34.0477
	MSR	5.319	0.5585	0.04	7.5753	22.3488	26.9719
	MSRACE	5.1412	0.5239	0.0118	7.4997	10.75	25.3848
	FLM	4.8002	0.5303	0.0684	7.2834	25.507	22.758
	LSCN	5.166	0.6268	0.096	7.509	**28.9555**	28.768
	JEI	5.55	0.6334	0.0231	7.777	13.2097	33.1123
	MDE	5.1367	0.5185	0.0097	7.4207	8.5504	29.8314
	PROPOSED	**5.7751**	**0.6479**	**0.1049**	**7.8992**	25.5165	**37.2033**

Table 9
Performance comparison of different enhancement techniques for image 9.

Image	Algorithm	Metrices					
		NIQMC	**BIQME**	**MICHELSON**	**DE**	**EME**	**PIXDIST**
IMG 9	BPDFHE	5.2581	0.5617	0.0618	7.3055	21.7543	26.5299
	DWT-SVD	5.3539	0.6161	0.0311	7.4381	13.7013	**42.508**
	RHE-DCT	5.4141	0.5903	0.0729	7.4827	24.7008	29.7896
	DRAGO	5.2304	0.5223	0.0079	7.4991	8.2202	29.3854
	DURAND	2.5138	0.2897	0.0021	5.3427	4.4484	9.2974
	FATTAL	5.2538	0.5309	0.0274	7.5017	12.7793	25.7331
	LCC	5.2861	0.5723	0.0365	7.2827	24.7994	24.3869
	MAI	5.7843	0.6089	0.0543	7.4361	18.8063	36.5379
	MSR	5.5844	0.5399	0.0471	7.5434	21.8008	29.7301
	MSRACE	5.5456	0.5567	0.0254	7.5997	13.5476	30.1091
	FLM	5.3229	0.567	0.0951	7.5936	30.9848	30.036
	LSCN	5.4821	0.5941	**0.1763**	7.492	**48.6581**	29.8053
	JEI	5.6593	0.636	0.0542	7.7842	18.749	34.3397
	MDE	5.6322	0.6255	0.0475	7.7024	13.741	37.4687
	PROPOSED	**5.7913**	**0.644**	0.1463	**7.885**	36.098	37.2709

2.2. Modified Linking Synaptic Computation Network (MLSCN)

Leaky integrators consist of membrane potential, linking synapse and the threshold, which are included as the building blocks of a linking synaptic network (Eckhorn et al., 1990; Johnson and Ritter, 1993; Johnson et al., 1999; Johnson and Padgett, 1990). The proposed enhancement method uses a modified and more adaptive version of LSCN. The modified linking synapse is mathematically formulated as in Eq. (3).

$$S_{i,j}(n) = lS_{i,j}(n-1) + \sum_{p,q} X_{i,j,p,q} Z_{p,q}(n-1) \tag{3}$$

where indices (i,j) denotes each neuron and indices (p,q) indicates its neighboring neuron, the linking constant is represented by l, $X_{i,j,p,q}$ represents the synaptic weight that is needed to be applied and $Z_{p,q}$ is the postsynaptic action potential. The index 'n', denotes the discrete time.

The feedback and feed forward components are fused together to produce the membrane potential (Eckhorn et al., 1990; Abbott and Regehr, 2004; Brosch and Neuman, 2014) and the modified membrane potential is given in Eq. (4)

$$W_{i,j}(n) = g\ \ W_{i,j}(n-1) + G_{i,j}(1 + \alpha\ \ S_{i,j}(n)) \tag{4}$$

where g represents the membrane potential attenuation constant and it is It is set a small value (i.e. 0.01) because the stable value should be less than initialized threshold. $G_{i,j}$ represents the normalized image as described earlier and α is the linking strength. The modified threshold is deduced from the neuron analog (French and Stein, 1970). The threshold of a neuron is depicted by a leaky integrator (Eckhorn et al., 1990; French and Stein, 1970) and is given in Eq. (5)

$$D_{i,j}(n) = h\ \ D_{i,j}(n-1) + f\ \ Z_{i,j}(n-1) \tag{5}$$

where h denotes threshold attenuation constant which provides the required exponential delay between the successive spikes otherwise it will lead to multiple spikes between each iteration and quality of the resultant image will be hampered. Parameter 'f' denotes magnitude constant and its value is set to 0.001 for recording the firing rate preciously.

At the starting of network iteration, the threshold decays from the starting value $D_{i,j}(0)$ before the first spike occurs. The modified threshold of linking synaptic computation network is mathematically formulated in Eq. (6)

$$D_{i,j}(n) = h\ \ D_{i,j}(n-1) - \ \ \beta + f\ \ Z_{i,j}(n-1) \tag{6}$$

where β represents a small positive constant and it is set to $\frac{1}{255}$, so as to ensure that the dynamic range of the image lies in [0, 255].

In the network iteration, after the threshold is exceeded by the membrane potential, a spike is produced by the neuron which is indicated in Eq. (7)

$$Z_{i,j}(n) = \begin{cases} 1, & if \quad W_{i,j}(n) > D_{i,j}(n) \\ 0, & otherwise \end{cases} \tag{7}$$

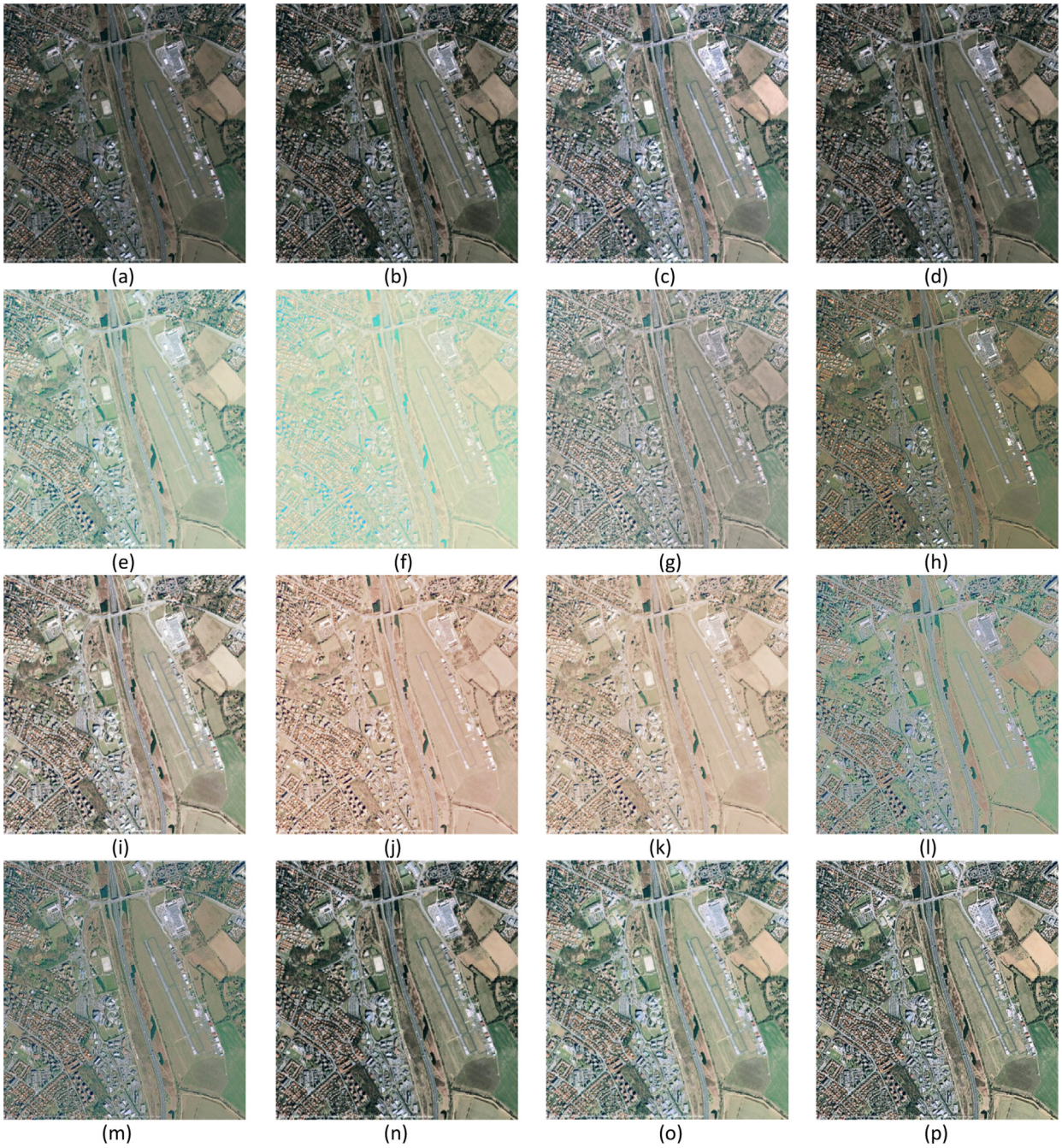

Fig. 3. Visual enhancement results of different algorithms for image 1. (a) given, (b) BPDFHE, (c) DWT-SVD, (d) RHE-DCT, (e) DRAGO, (f) DURAND, (g) FATTAL, (h) LCC, (i) MAI, (j) MSR, (k) MSRKACE, (l) FLM (m) LSCN, (n) JEI, (o) MDE, (p) PROPOSED.

The modified linking synaptic computation (MLSCN) is depicted in Eqs. (3), (4), (6) and (7). The schematic diagram of MLSCN is shown in Fig. 1. The MLSCN has two differences from LSCN (Zhan et al., 2017), the first is that the dynamic threshold which gives a better benchmark for the stimulus, and the second is that the input image is converted to mere stimulus for this network to work on.

2.3. Modified contrast enhancement algorithm using saliency map

The processed image from previous step is then enhanced using a modified contrast enhancement algorithm which uses a contrast map to improve its contrast. This modified technique mainly focuses on the contrast enhancement of the Linking Synapse stimulus. The processed stimulus may contain uneven low and dark regions. These regions are further improved in the forthcoming steps, which are as follows:

2.3.1. Stimulus lightness

In saliency guided enhancement algorithm, the lightness constituent of input RGB image is obtained and processed (Li et al., 2016). Whereas, the proposed method acquire the lightness constituent from the linking synapse obtained from Eq. (3) and is depicted in Eq. (8) (Li et al., 2016).

$$I_{i,j} = \max \; S_{i,j} \tag{8}$$

where $S_{i,j}$ denotes the output of the modified linking synapse and subscripts (i, j) denotes pixel indices. This technique is mainly helpful in transcending of the white balance.

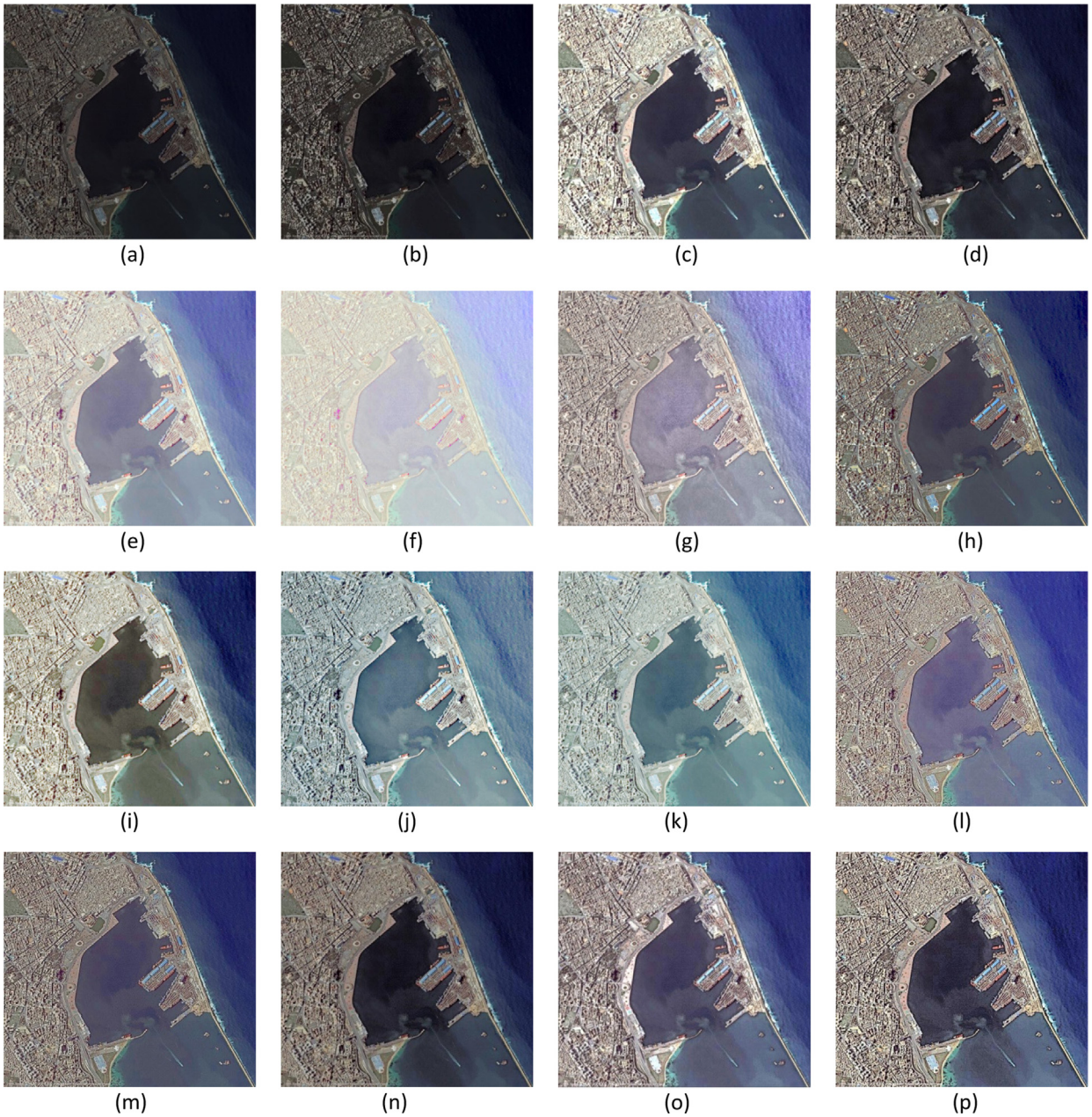

Fig. 4. Visual enhancement results of different algorithms for image 2. (a) given, (b) BPDFHE, (c) DWT-SVD, (d) RHE-DCT, (e) DRAGO, (f) DURAND, (g) FATTAL, (h) LCC, (i) MAI, (j) MSR, (k) MSRKACE, (l) FLM (m) LSCN, (n) JEI, (o) MDE, (p) PROPOSED.

2.3.2. *Bright region enhancement*

The output produced from previous section consists of both bright and dark regions. Here, we perform the contrast enhancement of bright region preserving the image details (Li et al., 2016). It is most probably difficult to reacquire much needed information from saturated regions, and most of the details which are remaining will be on the lower intensity side (Li et al., 2016). This amplitude of those will then become comparable to the noise level. Hence, it is essential for bright region enhancement for natural improvement of local contrast preventing halo artifacts without compromising the details (Li et al., 2016). The gain factor at pixel (i,j) for preserving bright regions details is given as in Eq. (9) [28].

$$k_{i,j} = 0.1 \times \sqrt{(dev_{i,j})_{5\times 5}} \tag{9}$$

where $(dev_{i,j})_{5\times 5}$ is the local standard deviation of a 5×5 neighbor window centered at (i, j).

The scene reflectance renders details following Eq. (10) (Li et al., 2016).

$$SC = \frac{I}{L + c} \tag{10}$$

where L is the illumination component same as the mean luminance value of the synaptic output and c is small constant to avoid zero division.

The details of bright regions are given as in Eq. (11) (Li et al., 2016).

$$B_{en} = SC^{k} \tag{11}$$

Here, the factor 'k', is the gain factor and it in defined in Eq. (9). It is obvious that these details have dispensable halo artifacts and clipping effects (Li et al., 2016). So, to remove them a tune mapping function is proposed, as a result of which the contrast of bright regions can be enhanced and it is indicated in Eq. (12) (Li et al., 2016).

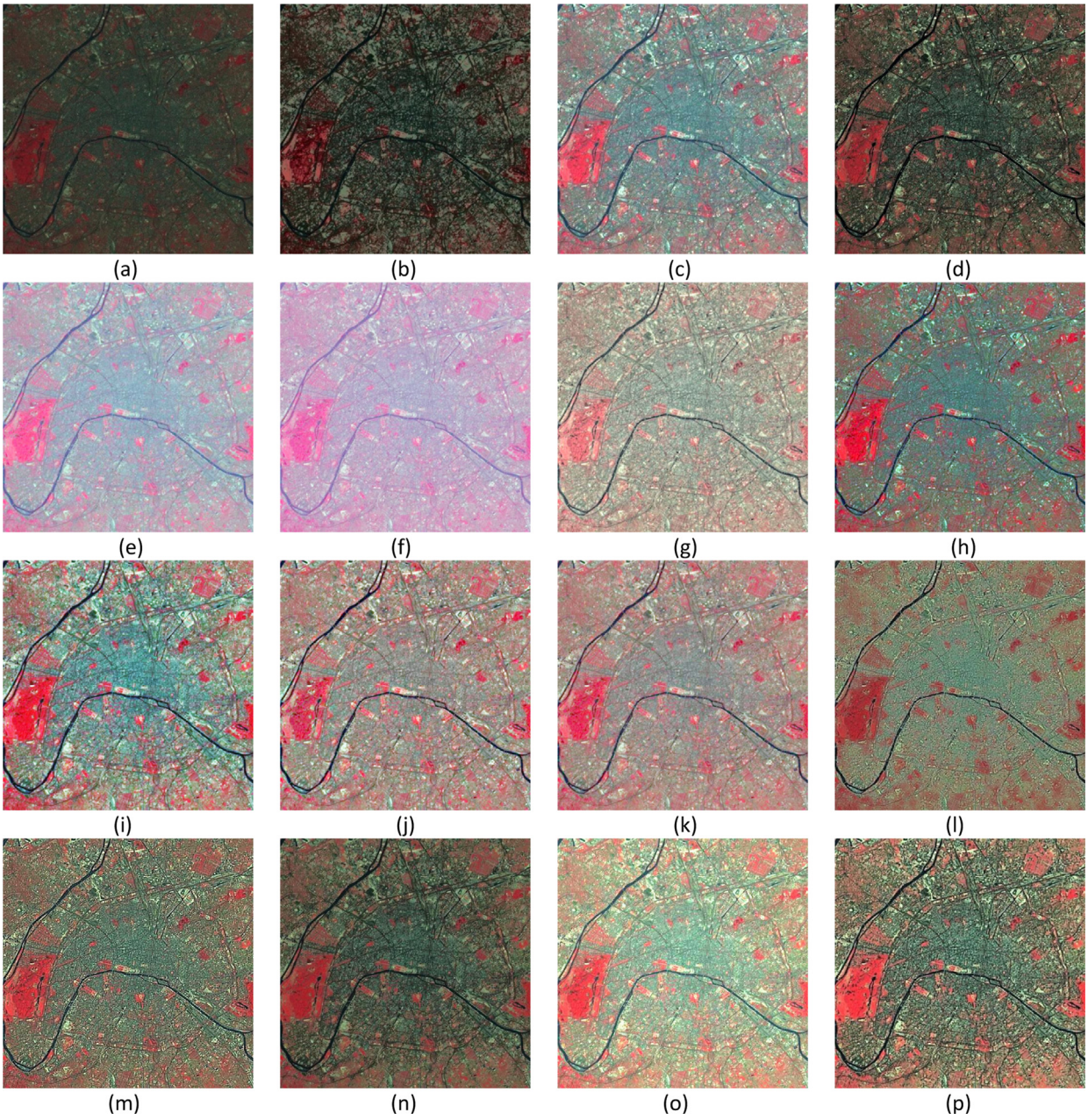

Fig. 5. Visual enhancement results of different algorithms for image 3. (a) given, (b) BPDFHE, (c) DWT-SVD, (d) RHE-DCT, (e) DRAGO, (f) DURAND, (g) FATTAL, (h) LCC, (i) MAI, (j) MSR, (k) MSRKACE, (l) FLM (m) LSCN, (n) JEI, (o) MDE, (p) PROPOSED.

$$I_{bright\,.\,en} = I^{B_{en}} \tag{12}$$

The preservation of details during the enhancement of contrast of bright regions and mid-tune range is ensured by tune mapping factor.

2.3.3. Dark region enhancement

The dark regions are left unchanged during bright region contrast enhancement procedure because of low lightness. A perceptual contrast map (*PC*) based on the modified difference of Gaussian is used for the extraction of edge contents (Li et al., 2016; Zang et al., 2013). The amplitude of the *PC* indicates the information strength in the frequency. The construction process of perceptual contrast map consists of central component (in a $(2k_C + 1) \times (2k_C + 1)$ central mask) $(K_C)_{i,j}$ and surrounding component (in a $(2k_S + 1) \times (2k_S + 1)$ surround mask) $(K_S)_{i,j}$ is given by,

$$(K_C)_{i,j} = \sum_{x\,=\,i-k_C}^{x\,=\,i+k_C} \sum_{y\,=\,j-k_C}^{y\,=\,j+k_C} (CGE)_{x-i,y-j} \quad S_{x,y} \tag{13}$$

$$(K_s)_{i,j} = \sum_{x\,=\,i-k_s}^{x\,=\,i+k_s} \sum_{y\,=\,j-k_s}^{y\,=\,j+k_s} (SGE)_{x-i,\,y-j} \quad S_{x,y} \tag{14}$$

where $S_{i,j}$ is the linking synaptic output, $k_C = 1$, $k_S = 0.01 \times \min(h, w)$; where (h, w) denotes the height and width of the image; $(CGE)_{i,j}$ and $(SGE)_{i,j}$ are the two Gaussian functions which are mathematically defined in Eq. (15) and Eq. (16) respectively.

$$(CGE)_{i,j} = \exp\left[-\left(\frac{3i}{k_C}\right)^2 - \left(\frac{3j}{k_C}\right)^2\right] \tag{15}$$

$$(SGE)_{i,j} = 0.85\left(\frac{k_C}{k_S}\right)^2 \exp\left[-\left(\frac{3i}{k_S}\right)^2 - \left(\frac{3j}{k_S}\right)^2\right] \tag{16}$$

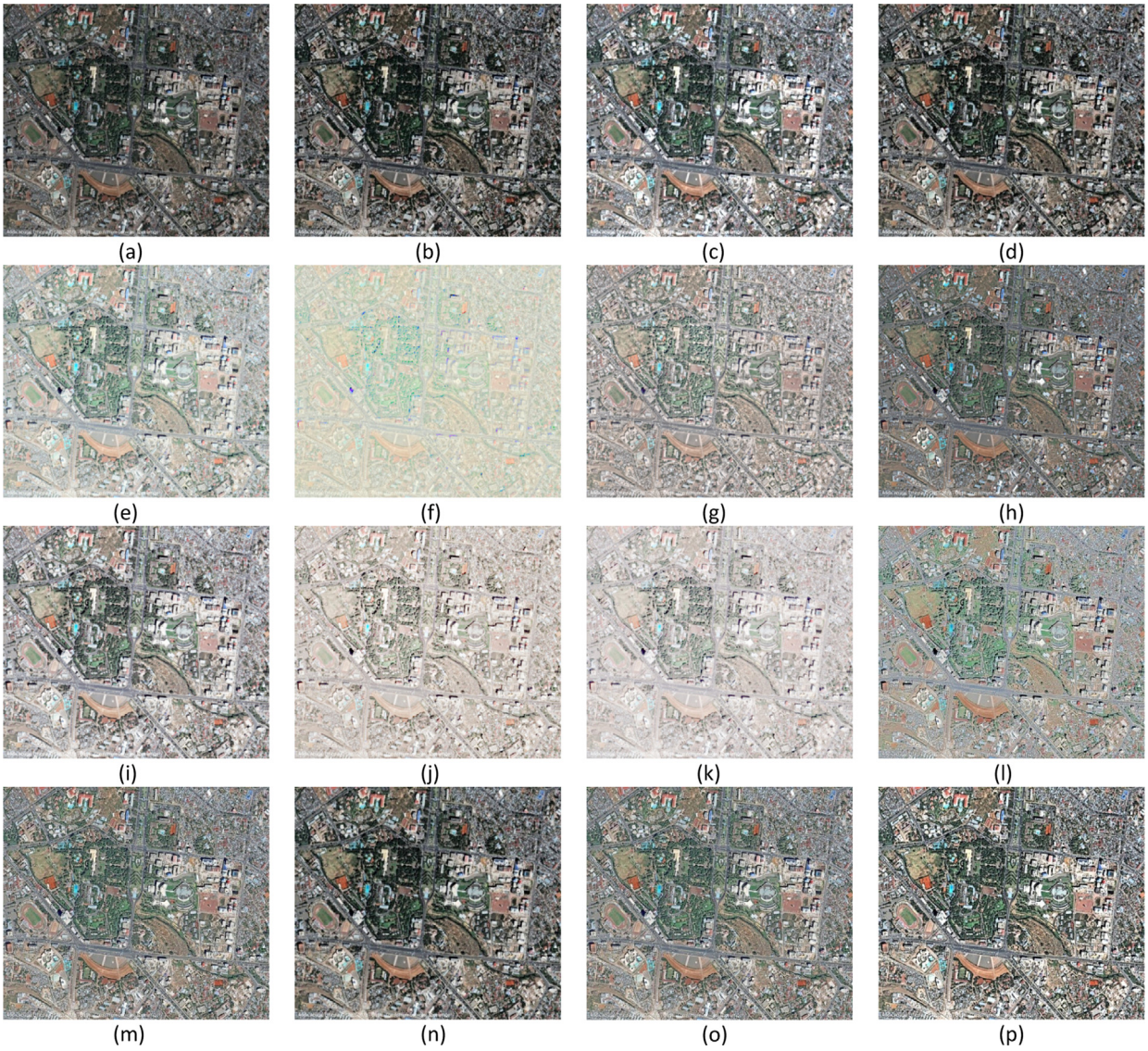

Fig. 6. Visual enhancement results of different algorithms for image 4. (a) given, (b) BPDFHE, (c) DWT-SVD, (d) RHE-DCT, (e) DRAGO, (f) DURAND, (g) FATTAL, (h) LCC, (i) MAI, (j) MSR, (k) MSRKACE, (l) FLM (m) LSCN, (n) JEI, (o) MDE, (p) PROPOSED.

The synaptic output image is conditioned by the mathematical Eq. (17)

$$C_{i,j} = I_{i,j}|(PC)_{i,j}|, \tag{17}$$

where PC is defined as $(PC)_{i,j} = \frac{(K_C)_{i,j} - (K_S)_{i,j}}{(K_S)_{i,j}}$

The conditioned image is normalized to C_{nor} using the maximum and minimum values of C. The perceptual contrast improvement of dark region is calculated and the modified image is represented as $I_{perceptual,en}$(Li et al., 2016).

Then, the $I_{bright.en}$ and $I_{perceptual,en}$ are blended under saliency guide to produce more natural and contrast enhanced image and is given as

$$(I_{en})_{i,j} = (C_{nor})_{i,j}\ I_{bright.en} + (1 - (C_{nor})_{i,j})\ \ I_{perceptual.en} \tag{18}$$

Thus, the final output of this modified contrast enhancement with color correction method is given in Eq. (19).

$$r = \frac{I_{en}}{I} \tag{19}$$

This color correction is applied to HSV model given in the input and converted to the RGB form and is then applied to a modified natural color restoration algorithm.

2.4. Efficient color restoration

The RGB image from the previous step is passed for an efficient color restoration technique with non-uniform illumination enhancement to overcome any problem for color violation (Jmal et al., 2017). It employs an optimized search process based on an efficient search algorithm for computing optimal parameters resulting the final enhanced image (Jmal et al., 2017).

2.5. Implementation of proposed framework

The workflow diagram of proposed image quality restoration framework for contrast enhancement for satellite images is shown in Fig. 2. The detailed implementation steps and procedures followed by the proposed image quality restoration framework are as follows:

Step 1: Smoothing and Edge Enhancement effect: This can be considered as the first step of image enhancement, which mainly focuses on improving the edges. It also includes the initialization of variables to be used in the later steps. After the conversion of the RGB input to HSV, it is converted into a double symmetric array. This is followed by normalization and smoothening using guided filter and the

Fig. 7. Visual enhancement results of different algorithms for image 5. (a) given, (b) BPDFHE, (c) DWT-SVD, (d) RHE-DCT, (e) DRAGO, (f) DURAND, (g) FATTAL, (h) LCC, (i) MAI, (j) MSR, (k) MSRKACE, (l) FLM (m) LSCN, (n) JEI, (o) MDE, (p) PROPOSED.

edge enhanced output is obtained as defined in Eq. (2).

Step 2: **Modified Linking Synaptic Network using Leaky integrator:** After the image has been edge enhanced it comes to this step. This step is responsible for the conversion of the image into a better enhanced stimulus. This step begins with the formation of a linking synapse as depicted in Eq. (3). This is succeeded by a modified membrane potential as in Eq. (4). All these steps occurring in the network iteration, where total numbers of pixels mark the total number of iterations are provided with a threshold (as given in Eq. (6)) which when exceeded by the membrane potential generate a spike as explained in Eq. (7). This spike keeps on updating the linking synapse to give a final synaptic output which is similar to the stimulus received by the brain.

Step 3: Modified Contrast Enhancement Algorithm using Saliency Map: The synaptic output is passed for contrast enhancement where its lightness constituent is obtained as per Eq. (8). Here, in this step, the dark and bright regions are enhanced separately as depicted in Eqs. (12) and (17). For the bright region enhancement, a 5×5 window is defined and the gain factor is calculated by taking the standard deviation of this window using the Eq. (9). The details of these bright regions are formulated using Eq. (11), provided the scene reflectance is obtained using the Eq. (10). The dark region enhancement mainly focuses on highlighting the perceptually important local edges and reducing the larger frequency noises in smooth regions. This is done by taking two components i.e. central component and surround component and are operated taking their masks as depicted in Eqs. (13) and (14) respectively.

Step 4: Efficient Color Restoration: This step is the final step of the enhancement framework as it gives the required balance between the colors in the image so as to give a naturalistic view. This step preserves a reasonable degree of color constancy as described in the Section 2.

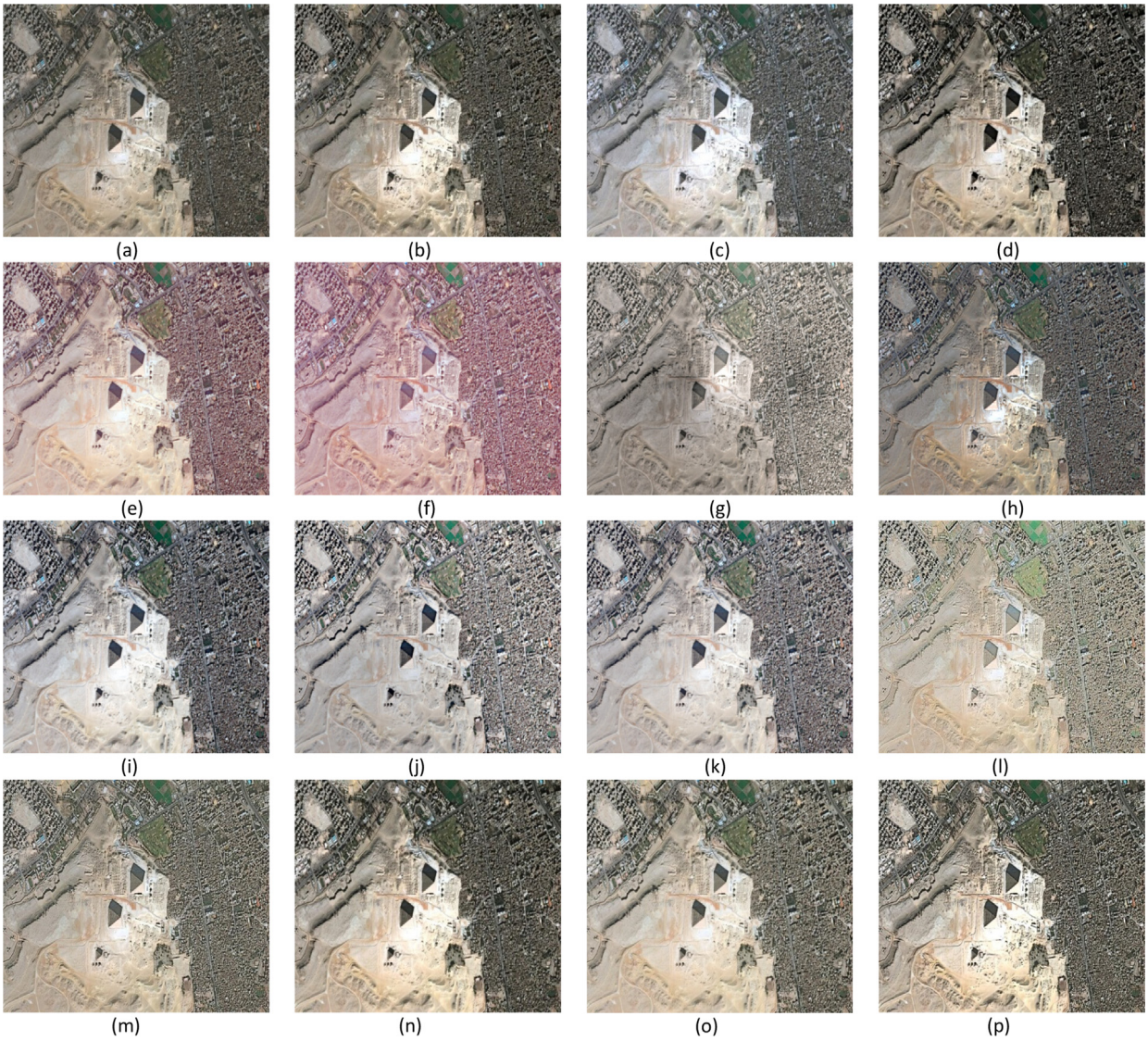

Fig. 8. Visual enhancement results of different algorithms for image 6. (a) given, (b) BPDFHE, (c) DWT-SVD, (d) RHE-DCT, (e) DRAGO, (f) DURAND, (g) FATTAL, (h) LCC, (i) MAI, (j) MSR, (k) MSRKACE, (l) FLM (m) LSCN, (n) JEI, (o) MDE, (p) PROPOSED.

3. Experimental results and discussion

Our method has been tested against a variety of algorithms over a handful of satellite remote sensing images. The algorithms included for comparison are Brightness Preserving Dynamic Fuzzy Histogram Equalization (BPDHE) (Sheet et al., 2010), Satellite Image Contrast Enhancement Using Discrete Wavelet Transform and Singular Value Decomposition (DWT-SVD) (Demirel et al., 2010), Regularized Histogram Equalization method and Discrete Cosine Transform (RHE-DCT) (Fu et al., 2015),Tone Mapping Methods like DRAGO (Drago et al., 2003; Lisani et al., 2016), DURAND (Durand and Dorsey, 2002; Lisani et al., 2016), FATTAL (Fattal et al., 2002; Lisani et al., 2016), LCC (Local Color Correction)(Moore et al., 1999; Lisani et al., 2016), MAI (Mai et al., 2011; Lisani et al., 2016) MSR (Multi-Scale Retinex) (Petro et al., 2014; Lisani et al., 2016), MSRKACE (Multi-Scale Retinex with ACE Kernel) (Morel et al., 2014; Lisani et al., 2016), Neurocomputing methods like FLM (Zhan et al., 2016, 2017; Li et al., 2017), LSCN (Zhan et al., 2017; Suresh and Lal, 2017; Li et al., 2017), a method of JEI (Jmal et al., 2017) and a Modified Differential Evolution (MDE) algorithm (Suresh and Lal, 2017). The values of the parameters used in these methods and algorithms are chosen from the respective literatures and those used in the proposed technique are derived by their working form. We set $\beta = \frac{1}{255}$, for obtaining a better dynamic range. It is a small constant and its value is set to $\frac{1}{255}$, so as to ensure that the dynamic range of the image lies in [0, 255]. The final linking state $S_{i,j}$ is greater for a single neuron having shorter firing cycle, so $l = 1$ is put for carrying out better firing rate of neurons. The synaptic Weight Matrix has its center element set to 1 and is given by,

$$X = \begin{bmatrix} 0.04 & 0.04 & 0.04 \\ 0.04 & 1 & 0.04 \\ 0.04 & 0.04 & 0.04 \end{bmatrix}$$

The linking term controls the degree of image smoothening so the synaptic weights other than center are set to 0.04 The parameter 'g' which is the membrane potential attenuation constant is set a small value 0.01 because the stable value should be less than initialized threshold (Zhan et al., 2017). The parameters h, α (The membrane potential has linking term which is a weak modulation term) and f (for precious recording of the firing rate) are set to be 0.9811, 0.01 and 0.001 respectively for ensuring better performance of our proposed method. The Parameter 'α ' is the linking strength and it is assumed a small value. This is because membrane potential contributes to stimulus and for membrane potential, linking term is weak modulation term (Eckhorn et al., 1990; Abbott and Regehr, 2004; Brosch and Neuman,

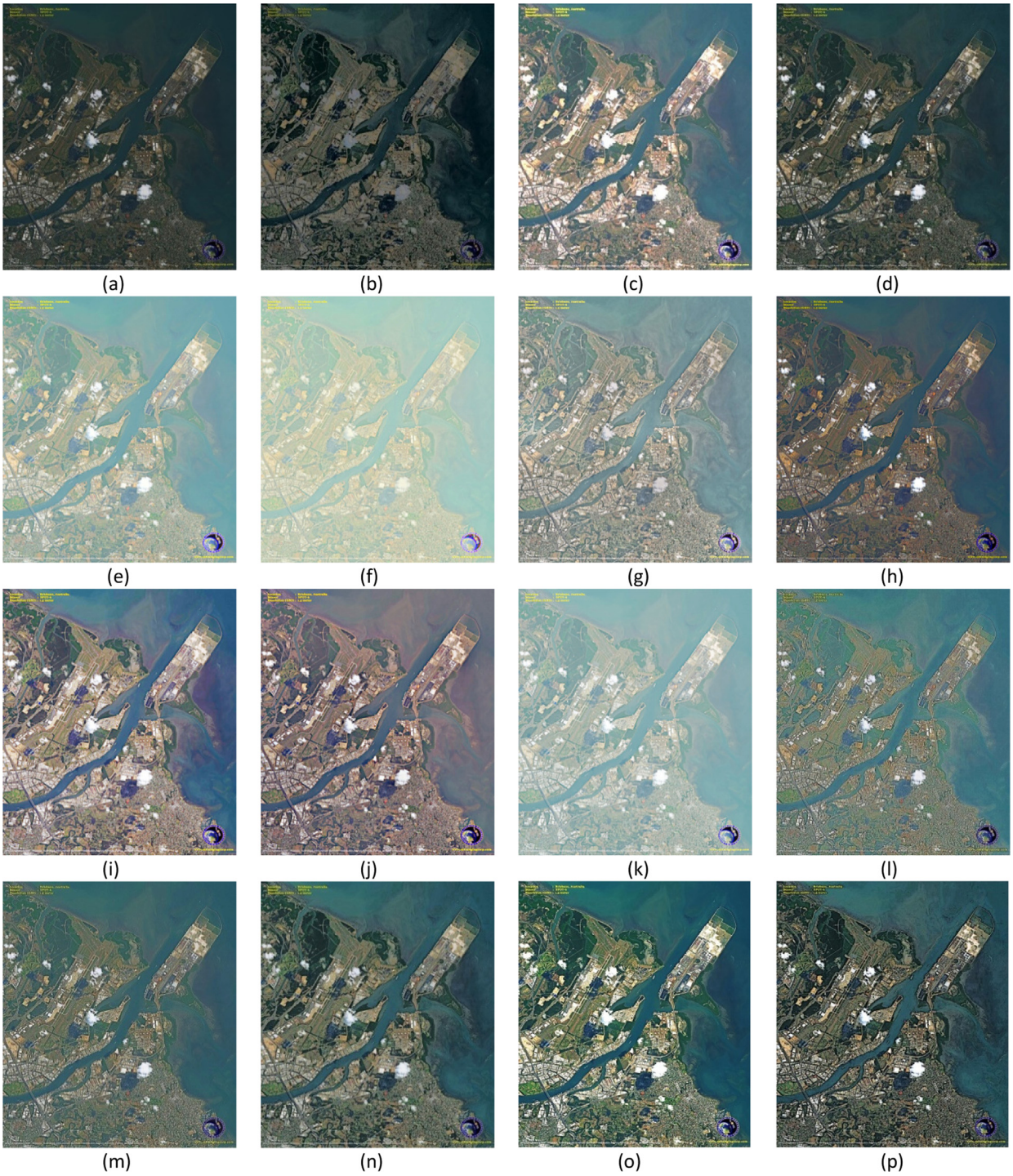

Fig. 9. Visual enhancement results of different algorithms for image 7. (a) given, (b) BPDFHE, (c) DWT-SVD, (d) RHE-DCT, (e) DRAGO, (f) DURAND, (g) FATTAL, (h) LCC, (i) MAI, (j) MSR, (k) MSRKACE, (l) FLM (m) LSCN, (n) JEI, (o) MDE, (p) PROPOSED.

2014; Zhan et al., 2017).. The parameter '*h*' is the threshold attenuation constant which provides the required exponential delay between the successive spikes otherwise it will lead to multiple spikes between each iteration and quality of the resultant image will be hampered. Parameter 'f' is magnitude constant and it's value is set to 0.001 $\left(<\frac{1}{255}\right)$ for recording the firing rate preciously The total number of neurons to be fired for a selected image of size $a \times b$, is $a * b$.

3.1. Satellite image datasets

For the simulation experiments, the different test satellite images used were those procured from different sensors (i.e. SPOT, IKONOS, MODIS and QUICKBIRD). The specifications and sources of various test images used in this paper are Image1: City of Space Toulouse, France (1200 × 1200, MS (Multispectral), 50 cm resolution, SPOT data, http://www.satpalda.com/gallery/pleiades-imagery/); Image2: Tripoli Harbour, Libya, (900 × 792, MS, 50 cm resolution, SPOT data, http://www.satpalda.com/gallery/pleiades-imagery/); Image3: Seine river, Paris (512 × 512, MS, 50 cm resolution, IKONOS data, http://

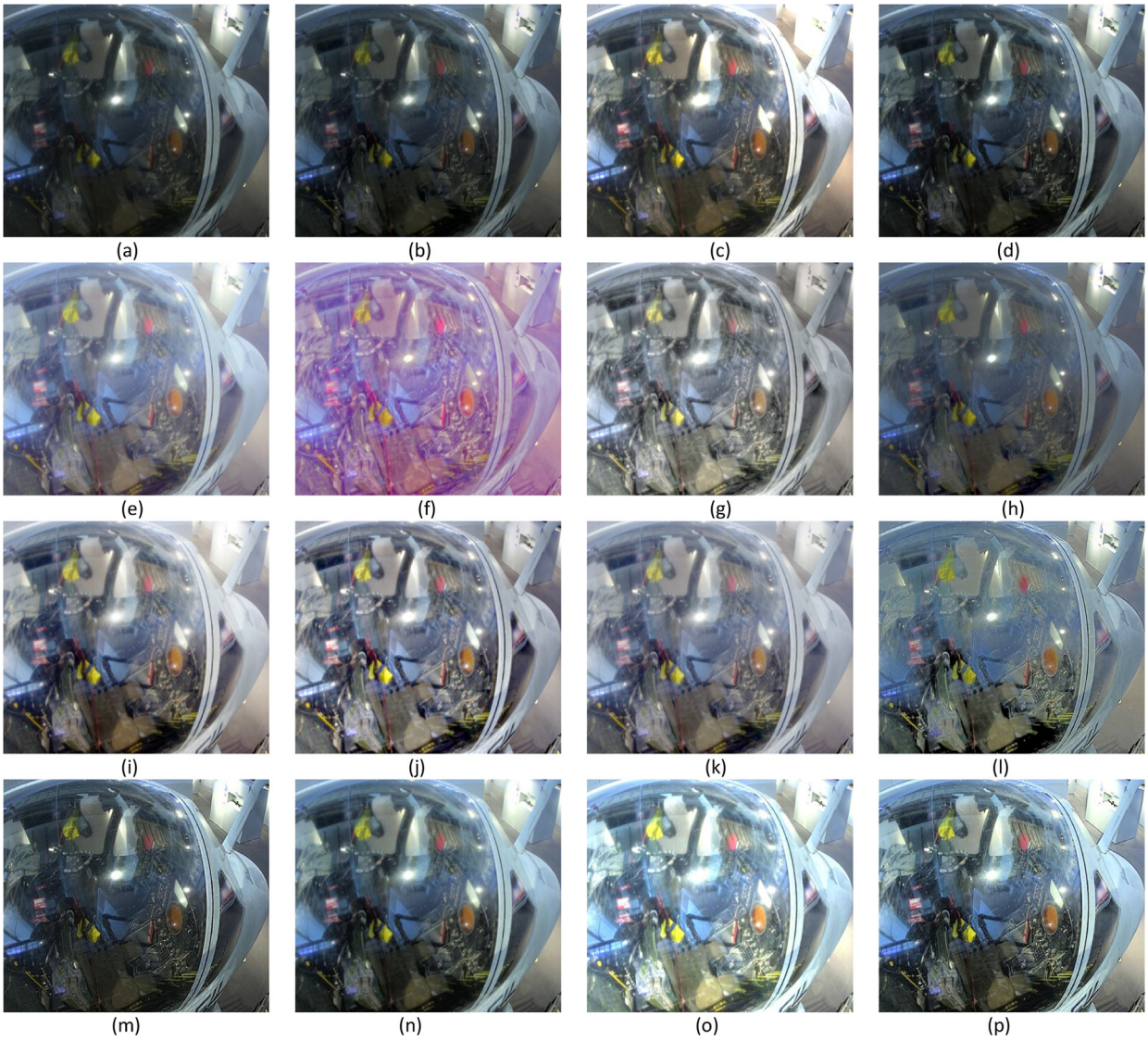

Fig. 10. Visual enhancement results of different algorithms for image 8. (a) given, (b) BPDFHE, (c) DWT-SVD, (d) RHE-DCT, (e) DRAGO, (f) DURAND, (g) FATTAL, (h) LCC, (i) MAI, (j) MSR, (k) MSRKACE, (l) FLM (m) LSCN, (n) JEI, (o) MDE, (p) PROPOSED.

visibleearth.nasa.gov/); Image4: Addis Ababa, Ethiopia (900 × 702, MS, 50 cm resolution, SPOT data, http://www.satimagingcorp.com/gallery/); Image5: Lightning Fires in Central Idaho (1800 × 2400, MS, 50 cm resolution, MODIS data, http://earthobservatory.nasa.gov/) and Image6: Pyramids, Egypt (900 × 607, MS, Quickbird data, http://www.satpalda.com/gallery/pleiades-imagery/). Image 7: 793 × 624, MS, http://www.satimagingcorp.com/gallery/; Image 8, 1312 × 2000,natural images, http://dragon.larc.nasa.gov/retinex/; Image 9, 624 × 491, natural image, http://dragon.larc.nasa.gov/retinex/.

3.2. Quantitative result analysis

The quantitative assessments are used to appraise and compare the aforementioned remote sensing enhancement methods and algorithms with the proposed method for satellite image enhancement. The quantitative performance assessments are done using the help of six No Reference (NR) performance metrics. It includes No Reference Image Quality Metric for Contrast distortion (NIQMC) (Gu et al., 2017) based on information maximization, Blind Image Quality Measure of Enhanced images (BIQME) (Gu et al., 2018) based on a measure of visual quality and learning with big data training samples, Michelson Contrast (MICHELSON) (Michelson, 1995), Discrete Entropy (DE) (Shannon,1948; Shin and Park, 2015), measure of enhancement (EME) (Agaian et al., 2007) and Pixel distance (PIXDIST) (Chen et al., 2006a; Chen et al., 2006b). Higher its value, better the image enhancement method used. Tables 1–9 depicts the evaluated quality metric values for all the image enhancement algorithms compared, for the six test images included in the study. Comparison of performance metrics for Images 1–4 and 7 indicates the quality parameters of proposed method to take a decent upper hand over other existing remote sensing enhancement methods. Whereas for Images 5–6, 8 and 9 the evaluated metrics, especially EME, shows slight discrepancy in their performance. Nevertheless, the overall qualitative analysis done on the set of test satellite images, as given in Tables 1–9, indicates that the proposed method outperforms the other 14 existing remote sensing enhancement methods clearly.

3.3. Qualitative result analysis

We analyzed the proposed method against other existing enhancement methods such BPDHE, DWT-SVD, RHE-DCT, DRAGO DURAND, FATTAL, LCC, MAI, MSR, MSRKACE, FLM, LSCN, JEI and MDE qualitatively on six satellite remote sensing images. The qualitative results of

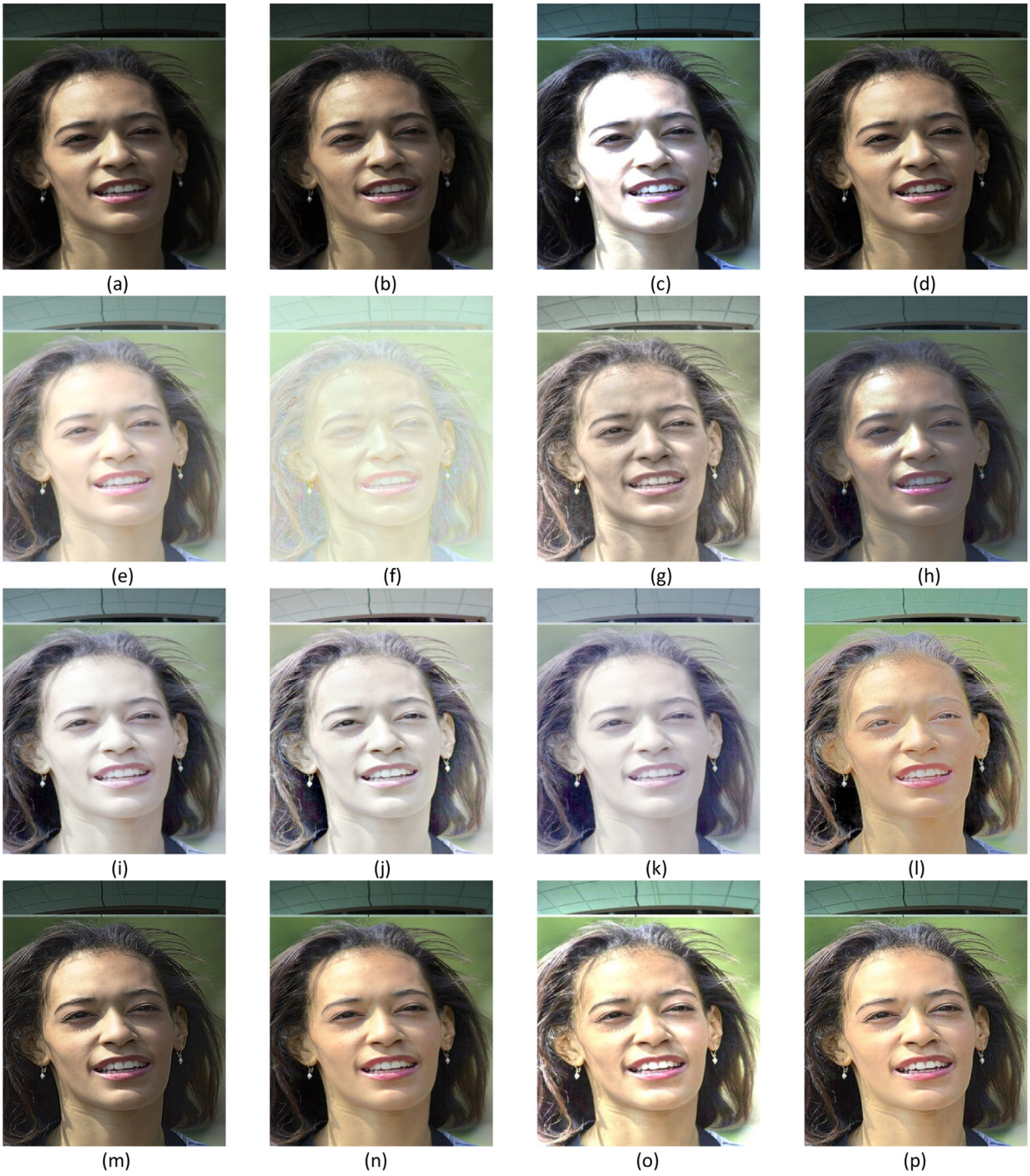

Fig. 11. Visual enhancement results of different algorithms for image 9. (a) given, (b) BPDFHE, (c) DWT-SVD, (d) RHE-DCT, (e) DRAGO, (f) DURAND, (g) FATTAL, (h) LCC, (i) MAI, (j) MSR, (k) MSRKACE, (l) FLM (m) LSCN, (n) JEI, (o) MDE, (p) PROPOSED.

proposed method and other existing remote sensing enhancement methods are given in Figs. 3–11. Visual enhanced result of BPDFHE method introduced some unpleasant saturation effect. This leads to unclear gradients which imply that the local details are not enhanced enough. Whereas, DWT-SVD method resulted in good contrast but other image details are not clear. There is also dearth of natural color in the enhanced images because the DWT-SVD method only focuses on the low–low sub band images and overlooks the high-frequency parts. The enhanced image using RHE-DCT method resulted in quite under enhanced and unclear image details. The darker region remains dark and the brighter regions are slightly enhanced. DRAGO method introduced too much intensity boost as a result of excessive enhancement and hence processed image become whiter. Similarly, DURAND method also made the processed image even more whitish because of over saturation effects. The FATTAL enhancement method introduced blurring as well as over saturation ill effects. The LCC method made the images appear slightly smoothed and also displayed some unnatural appearance. But, it suffers from lesser over enhancement problems as compared with the previous two. The visual enhanced result of MAI method also resulted in an unnatural processed image. Whereas, MSR method resulted in decolorized images and the processed images appeared faded out, due to the fact that it focused on detailed enhancement at the

Table 10
CPU runtime of different image enhancement algorithms (in second).

Image	Algorithm					
	RHE-DCT	FLM	LSCN	JEI	MDE	Proposed
Image 1	1.4931	4.8116	25.0595	2.4303	223.9377	6.7307
Image 2	0.5812	1.8636	7.008	0.8486	195.4553	2.4948
Image 3	0.4732	1.3856	5.0739	0.6797	169.4950	1.8060
Image 4	1.1175	3.5255	16.3456	1.6914	212.1176	4.9464
Image 5	1.0849	3.7415	13.5184	4.0012	203.5848	4.1987
Image 6	0.6105	1.6779	6.3337	0.7757	183.4013	2.3156
Image 7	1.8112	3.6784	14.4912	1.0422	844.2373	5.2891
Image 8	1.4022	1.8380	5.4941	0.7281	457.6354	3.2547
Image 9	1.1654	1.8016	7.7032	0.8583	449.7132	3.4694

expense of natural color. The enhancement result of MSRKACE method also resulted in a similar decolorized and faded image output. FLM method resulted in over smoothening of edges along with saturation ill effects. The LSCN method provided lesser enhancement with loss of details at the edges. It also resulted in slightly faded colors in the processed image. The use of high pass filter in LSCN method also resulted in the magnification of noisy pixels introducing small ringing effect. The visual enhanced result of JEI method provided better display of the details and colors except in low lighted regions. Whereas, the most recent MDE algorithm for satellite image enhancement, provided a decent output, but resulted in over smoothening of fine edges and features in the processed image. Finally, on comparison with the other 14 state-of-the art algorithms, the proposed method provided high global contrast preserving local details and edges. The local details were well emphasized and the corresponding gradients as well as textures were relatively clearer. Hence, the proposed method ensured a decent trade-off between the contrast enhancement, luminance acclimation and preservation of details and natural color.

3.4. Comparison of Computational Cost

The runtime for various algorithms is depicted in Table 10. The proposed method requires slightly longer time than, RHE-DCT, FLM and JEI. The RHE-DCT method takes least time than other methods because it is a histogram based technique and its implementation is simple. The evolutionary algorithm based MDE method is slowest compared to the other methods. Our method is implemented in MATLAB R2015a running on an Intel Core i5 − 4210U Laptop with 1.7-GHz CPU, 8-GB RAM, and 64-bit operating system. It can be further proliferated faster using faster programming languages and computing devices such as GPU.

4. Conclusion

In this paper, a robust framework for contrast enhancement of satellite images was proposed. The enhancement process was designed based on a modified linking synaptic network blended with saliency map for better visibility of the dark details. Secondly, the naturalness of the image is preserved with halo artifacts suppression using the image restoration technique. To measure the robustness of the proposed enhancement method, the performance evaluation was conducted on a wide range of remote sensing databases in terms of NIQMC, BIQME, MICHELSON, DE, EME and PIXDIST. The results were also compared with state-of-the-art contrast enhancement algorithms. Visual comparison of the experimental results proved that the proposed enhancement method to be a clear winner among others in enhancing the contrast without compromising the naturalness of the images. Quantitative evaluation provided ample evidences to judge the proposed method to be the most efficacious among the set of compared enhancement algorithms. Comparison of execution time also revealed the proposed method to be computationally efficient in the process of satellite image enhancement. The advantages of proposed method are (1) Robustness and (2) less computational complexity as compared to recent existing remote sensing contrast enhancement methods. The main disadvantages of proposed method is litter more processing as compared to some existing remote sensing enhancement methods. It also leaves an opportunity for its future usability in the pre-processing stages of various image applications.

Acknowledgement

The authors would like to thank the editors and anonymous reviewers for their valuable suggestions and comments which helped to improve the quality of the research paper. Author also would like to thank Prof. José Luis Lisani Roca, Department of Mathematics and Computer Science University of the Balearic Islands, Spain for providing processed results of remote sensing enhancement methods presented in his paper published in IEEE Journal of Selected Topics in Applied Earth Observations and Remote Sensing (JSTARS).

References

Abbott, L., Regehr, W., 2004. Synaptic computation. Nature 431 (7010), 796–803.
Agaian, S., Silver, B., Panetta, K., 2007. Transform coefficient histogram based image enhancement algorithms using contrast entropy. IEEE Trans. Image Process. 16 (3), 741–758.
Arici, T., Dikbas, S., Altunbasak, Y., 2003. A histogram modification framework and its application for image contrast enhancement. IEEE Trans. Image Process. 18 (9), 706.
Brosch, T., Neuman, H., 2014. Interaction of feed-forward and feedback streams in visual cortex in a firing-rate model of columnar computations. Neural Netw. 54, 11–16.
Celik, T., Tjahjadi, T., 2012. Automatic image equalization and contrast enhancement using Gaussian Mixture modelling. IEEE Trans. Image Process. 21 (1), 145.
Chen, Z., Abidi, B.R., Page, D.L., Abidi, M.A., 2006a. Gray-level grouping: an automatic method for optimized image-contrast Enhancement part 1: the basic method. IEEE Trans. Image Process. 15 (8), 2290.
Chen, Z., Abidi, B.R., Page, D.L., Abidi, M.A., 2006b. Gray-level grouping (GLG): an automatic method for optimized image contrast Enhancement-part I: the basic method. IEEE Trans. Image Process 15 (8), 2290–2302.
Cheng, G., Han, J., Guo, L., Liu, Z., Bu, S., Ren, J., 2015. Effective and efficient midlevel visual elements-oriented land-use classification using VHR remote sensing images. IEEE Trans. Geosci. Remote Sens. 53 (8), 4238–4249.
Demirel, H., Ozcinar, C., Anbarjafari, G., 2010. Satellite image contrast enhancement using discrete wavelet transform and singular value decomposition. IEEE Geosci. Remote Sens. Lett. 7 (2), 333–337.
Drago, F., Myszkowski, K., Annen, T., Chiba, N., 2003. Adaptive logarithmic mapping for displaying high contrast scenes. Comput. Graph. Forum 22 (3), 419–426.
Durand, F., Dorsey, J., 2002. Fast Bilateral filtering for the display of high dynamic range images. ACM Trans. Graph. 21 (3), 249–256.
Eckhorn, R., Reitboeck, H., Arndt, M., Dicke, P., 1990. Feature linking via synchronization among distributed assemblies: simulations of results from cat visual cortex. Neural Comput. 2 (3), 293.
Fattal, R., Lischinski, D., Werman, M., 2002. Gradient domain high dynamic range compression". ACM Trans. Graph. 21 (3), 249–256.
French, A.S., Stein, R.B., 1970. A flexible neural analog using integrated circuits. IEEE Trans. Biomed. Eng. BME-17 (3), 248–253.
Fu, X., Wang, J., Zeng, D., Huang, Y., Ding, X., 2015. Remote sensing image enhancement using regularized-histogram equalization and DCT. IEEE Geosci. Remote Sens. Lett. 12 (11), 2301–2305.
Gu, K., Lin, W., Zhai, G., Yang, X., Zhang, W., Chen, C.W., 2017. No-reference quality metric of contrast-distorted images based on information maximization. IEEE Trans. Cybern. 47 (12), 4559–4565.
Gu, K., Tao, D., Qiao, J., Lin, W., 2018. Learning a no-reference quality assessment model of enhanced images with big data. IEEE Trans. Neural Netw. Learn. Syst. 29 (4), 1301–1313. http://dx.doi.org/10.1109/TNNLS.2017.2649101.
He, K., Sun, J., Tang, X., 2013. Guided Image Filtering. IEEE Trans. Pattern Anal. Mach. Intell. 35 (6), 1397–1409.
Jmal, M., Souidene, W., Attia, R., 2017. Efficient Cultural heritage image restoration with nonuniform illumination enhancement. J. Electron. Imaging 26 (1) (011020–011020).
Johnson, J.L., Padgett, M.L., 1990. PCNN models and applications. IEEE Trans. Neural Netw. vo. 10 (3), 480.
Johnson, J.L., Ritter, D., 1993. Observation of periodic waves in a pulse-coupled neural network. Opt. Lett. 18 (15), 1253.
Johnson, J.L., Taylor, J.R., Anderson, M., 1999. Pulse-coupled neural network shadow compensation. Proc. SPIE 3722, 452.
Li, L., Si, Y., Jia, Z., 2017. Remote sensing image enhancement based on non-local means filter in NSCT domain. Algorithms 10 (116), 1–13.
Li, Y., Zhanga, H., Jia, W., Yuana, D., Chenga, F., Jia, R., Li, L., Sun, M., 2016. Saliency guided naturalness enhancement in color images. Optik 127, 1326–1334.
Lisani, J.L., Michel, J., Morel, J.M., Petro, A.B., Sbert, C., 2016. An inquiry on contrast

enhancement methods for satellite images. IEEE Trans. Geosci. Remote Sens. 54 (12), 7044–7054.
Mai, Z., Mansour, H., Mantiuk, R., Nasiopoulos, P., Ward, R., Heidrich, W., 2011. Optimizing a tone curve for backward compatible high dynamic range image and video compression". IEEE Trans. Image Process. 20 (6), 1558–1571.
Michelson, A., 1995. Studies in Optics. Courier Corp., New York, NY, USA.
Moore, A., Allman, J., Goodman, R.M., 1999. A real-time neural system for color constancy". IEEE Trans. Neural Netw. 2 (2), 237–246.
Morel, J., Petro, A., Sbert, C., 2014. What is the right center/surround for retinex? Process. ICIP 4552–4556.
Mukherjee, J., Mitra, S.K., 2008. Enhancement of color images by scaling the DCT coefficients. IEEE Trans. Image Process. 17 (10), 1783.
Petro, A.B., Sbert, C., Morel, J.M., 2014. Multiscale Retinex. Image Process. Line 4, 71–88.
Schowengerdt, R.A., 1997. Remote Sensing: Models and Methods for Image Processing, 2nd ed. Academic, New York, NY, USA.
Sen, D., Pal, S.K., 2011. Automatic exact histogram specification for image contrast enhancement, and visual system based quantitative evaluation. IEEE Trans. Image Process. 20 (5), 1211.
Shannon, C.E., 1948. A mathematical theory of communication. Bell Syst. Tech. J. 27 (3), 379–423.
Sheet, D., Garud, H., Suveer, A., Mahadevappa, M., Chatterjee, J., 2010. Brightness preserving dynamic fuzzy histogram equalization. IEEE Trans. Consum. Electron. 56 (4), 2475–2480.
Shin, J., Park, R.H., 2015. Histogram-based locality-preserving contrast enhancement. IEEE Signal Process. Lett. 22 (9), 1293–1296.
Starck, J., Murtagh, F., Candea, E.J., Donoho, D.L., 2003. Gray and color image contrast enhancement by curvelet transform. IEEE Trans. Image Process. 12 (6), 706.
Suresh, S., Lal, S., 2017. Modified differential evolution algorithm for contrast and brightness enhancement of satellite images. Appl. Soft Comp. 61, 622–641.
Tang, J., Kim, J., Peli, E., 2004. Image enhancement in the JPEG domain for people with vision impairment. IEEE Trans. Biomed. Eng. 51 (11), 2013.
Vadivel, A., Sural, S., Majumdar, A.K., 2005. Human color perception in the HSV space and its application in histogram generation for image retrieval. Proc. SPIE 5667, 598.
Wu, X., 2011. A linear programming approach for optimal contrast-tone mapping. IEEE Trans. Image Process. 20 (5), 1262.
Xu, H., Zhai, G., Wu, X., Yang, X., 2014. Generalized equalization model for image enhancement. IEEE Trans. Multimed. 16 (1), 68.
Zang, H., Li, Y., Chen, H., Yuan, D., Sun, M., 2013. Perceptual contrast enhancement with dynamic range adjustment. Optik 124, 5906–5913.
Zhan, K., Shia, J., Teng, J., Li, Q., Wang, M., Lu, F., 2017. Linking synaptic computation for image enhancement. Neurocomputing 238, 1–12.
Zhan, K., Teng, J., Shi, J., li, Q., Wang, M., 2016. Feature Linking Model for Image Enhancement. Letter. Neural Comput. 28, 1072–1100.
Zhan, K., Wang, H., Shi, J., Xie, Y., li, Q., 2017. Computational mechanisms of pulse coupled neural networks: a comprehensive review. Arch Comput. Methods Eng., Springer, 24(3), 2017, 573—588.
Zhang, F., Du, B., Zhang, L., 2015. Saliency-guided unsupervised feature learning for scene classification. IEEE Trans. Geosci. Remote Sens. 53 (4), 2175–2184.